EFFECTS OF ENVIRONMENTAL AND ELECTROCHEMICAL FACTORS ON THE LOCALIZED CORROSION OF ZIRCALOY-4

C.S. Brossia[1], C.A. Greene[2], D.S. Dunn[1], and G.A. Cragnolino[1]

[1]Center for Nuclear Waste Regulatory Analyses
Southwest Research Institute
6220 Culebra Road
San Antonio, TX 78238-5166

[2]US Nuclear Regulatory Commission
Washington, DC 20555-0001

ABSTRACT

Zircaloy-4 spent nuclear fuel cladding is considered by the U.S. Department of Energy as an additional metallic barrier for the containment of radionuclides in the proposed repository at Yucca Mountain. In this investigation, localized (pitting and crevice) corrosion of Zircaloy-4 is studied as a function of temperature (25 to 95 °C), chloride concentration (0.001 to 4.0 M), and pH (2.1 to 10.7) in solutions containing the predominant anions of the groundwater in the vicinity of the site to evaluate the behavior over a wide range of environmental conditions. Cyclic potentiodynamic polarization curves are used to determine the values of parameters, such as the repassivation potential for pitting corrosion, that can be used in performance assessment models. Corrosion potentials are determined on specimens covered with thermally grown oxide films to evaluate the possibility of localized corrosion under naturally corroding conditions inside breached containers for spent nuclear fuel. Electrochemical impedance spectroscopy (EIS) is used to study the properties of the passive and thermally grown oxide films.

Keywords: Zircaloy-4, pitting corrosion, crevice corrosion, pre-oxidation, oxide film resistance

INTRODUCTION

In order to meet the proposed Nuclear Regulatory Commission regulatory requirements contained in 10 CFR Part 63 [1]), U.S. Department of Energy must demonstrate that the annual expected dose to an average member of a receptor group located in the proximity of the proposed site from radionuclides released by spent nuclear fuel and high-level radioactive waste will not exceed 25 mrems within the 10,000-year regulatory time frame. The majority (65%) of the commercial spent nuclear fuel to be disposed in the proposed monitored geologic repository (MGR) at Yucca Mountain (YM), Nevada is clad with Zircaloy-4 (Zr-4) (UNS R60804). In addition, the commercial spent nuclear fuel accounts for 90% of the planned inventory in metric tonnes of heavy metal for the MGR. The U.S. Department of Energy in its recent performance assessment of the MGR has assumed that intact Zr-4 cladding is an additional metallic barrier to radionuclide release because the surface area of exposed irradiated UO_2 pellets is limited by breaches in the Zr cladding [2]. However, Zr and its alloys are known to be susceptible to various degradation modes as a result of aqueous corrosion that may lead to a premature failure of fuel cladding. One such mode is localized corrosion in the form of pitting corrosion. The purpose of this investigation was to examine the localized (pitting and crevice) corrosion behavior of Zr-4 under environmental conditions simulating those expected inside breached waste packages for spent nuclear fuel in the geologic repository.

Zr alloys, and in particular Zr-4, exhibit exceptional corrosion resistance in a variety of aqueous solutions over a wide range of pHs and temperatures due to the formation of a protective passive film composed of ZrO_2. The general aqueous corrosion of Zr-4 at temperatures up to 300 °C has been extensively investigated [3-5]. The protective oxide film growth rate is initially dependent on $(\text{time})^{-2/3}$, but undergoes a transition to a higher, approximately constant rate after some period of time. Breakdown of the oxide film formed during the fuel cycle under reactor operating conditions, followed by the initiation and

propagation of localized corrosion can significantly shorten the life of the nuclear fuel cladding once disposal containers are breached and modified groundwater penetrates the container.

Of the species expected to be present in the groundwater at YM, chloride and fluoride anions are considered to likely have the most significant effect on localized corrosion of Zr-4. Previous studies [6-12] have explored the effects of various chloride solutions on the localized corrosion of Zr and its alloys using electrochemical techniques. From these studies, as reviewed in more detail elsewhere [13], it can be concluded that pitting corrosion occurs in both neutral and acidic chloride solutions above a critical pit initiation potential for pitting initiation, which decreases linearly with the logarithm of the chloride concentration. The pitting potential measured by galvanostatic methods or potentiostatic techniques combined with mechanical disruption of the passive film by straining and scratching is very reproducible and coincides with the repassivation potential, E_{rp}, measured by slow, backward potential stepping or scanning once pitting corrosion is initiated. E_{rp} follows a linear logarithmic dependence on the chloride concentration similar to the well established expression for the pitting initiation potential found for other metals and alloys [14] according to Eq. (1),

$$E_{rp} = E^0_{rp} - B\log[Cl^-] \qquad (1)$$

where E^0_{rp} is the repassivation potential for a chloride concentration equal to 1 M. Values for B of 0.088 V/decade [10] and 0.080 V/decade [11] have been reported. Other authors, as recently reviewed (13), found a value of 0.059 V/decade, which corresponds to 2.303RT/F at 25 °C, as can be expected according to the model for pitting corrosion put forth by Galvele [15]. For Zr, a difference of approximately 40 mV between the values of E^0_{rp} at pH 0 and 5 was observed [11], whereas data from other authors have suggested that the value of E^0_{rp} is independent of pH within the range $0 < pH < 7$ and approximately equal

to 0.38 V_{SHE} [13]. For Zr-4, E^0_{rp} is equal to 0.34 V_{SHE} [8] and the decrease of 40 mV with respect to that of pure Zr is attributed to the effect of Sn as alloying element [6,8,13].

The objectives of this work are to evaluate the environmental and electrochemical conditions necessary for the occurrence of localized corrosion of Zr-4 in the proposed MGR, and to provide input to the fuel cladding degradation models to be used in predicting long-term material performance. This work will also lead to the development of methods appropriate for reviewing information the DOE is expected to provide in the licensing application.

EXPERIMENTAL PROCEDURES

All tests were performed using a single heat of Zr-4, whose chemical composition is shown in Table 1. Creviced specimens were constructed by pressing a serrated polytetrafluoroethylene (PTFE) crevice former, with a torque of 0.35 N·m, against the flat portion of a 1.9 × 1.9 × 1.3 cm (length × width × thickness) block specimen. Specimens were machined from an annealed 1.95 cm thick plate and wet polished to a 600 grit finish, cleaned and dried prior to assembling the crevice device inside the solution. Several specimens were oxidized in an air atmosphere at 200 °C for 9 or 56 days to study the effect of pre-formed oxide layer thickness on the corrosion behavior of Zr-4.

The tests were performed in chloride solutions in many cases (but not in all—see below) containing 0.25 mM sulfate (SO_4^{2-}), 0.16 mM nitrate (NO_3^-), 0.10 mM fluoride (F^-) and a total carbonate (HCO_3^- + CO_3^{2-}) concentration of 1.4 mM, in order to simulate the chemical composition of the prevalent ground water at the proposed MGR at YM. The chloride concentrations examined ranged from 1 mM to 4M. All solutions were prepared using reagent grade sodium salts and 18 MΩ·cm water. To modify the solution pH, 0.01 M HCl was added to lower the pH to 2.1 and Na_2CO_3 was used to raise the pH to 10.7.

Several tests were performed in chloride solutions without the addition of the other anions found in the groundwater. The tests were conducted at 25, 65, and 95 °C. After the bulk solution was prepared, the initial pH was measured at room temperature and the solution was introduced to the test cell. The solution was purged with high purity N_2 and heated to the desired temperature. The specimen was then introduced into the cell and the test was initiated after measuring the initial rest potential. After the test was completed, the final pH of the solution was measured at room temperature.

Cyclic potentiodynamic polarization (CPP) and potentiostatic tests were performed to examine the conditions under which localized corrosion of Zr-4 takes place. All tests were conducted using a saturated calomel reference electrode (SCE) maintained at room temperature and connected to the cell through a salt bridge/Luggin probe filled with either 100 mM or 1 M chloride solution depending on the concentration of the testing solution. A platinum foil was used as a counter electrode. CPP tests were initiated at 0.1 V less than the open circuit potential after the specimens had been immersed in the test solution and had reached a steady-state corrosion potential, E_{corr}. A potential scan rate of 0.167 mV/s was used and the scans were reversed when a current density of 5 mA/cm^2 was reached.

A series of open circuit potential measurements were also conducted to examine the possibility of exceeding the critical potentials for localized corrosion under naturally corroding conditions. These tests were performed in air-saturated solutions and involved the addition of hydrogen peroxide and ferric chloride to enhance the oxidizing power of the solution simulating the presence of radiolysis and corrosion products inside the disposal containers. In an attempt to explain differences in the open circuit behavior, the properties of the oxides formed at room temperature after polishing and, at 200 °C for 9 and 56 days were examined using electrochemical impedance spectroscopy (EIS). EIS was conducted in the passive range of the Zr-4 at -0.25 V_{SCE} in a deaerated, 10 mM NaCl solution at 25 °C using a 10 mV amplitude

sinusoidal potential wave. In addition, the relative electronic conductivity of these oxides were determined by comparing the anodic and cathodic current densities at overpotentials of +0.2 and -0.2 V relative to the specimen open circuit potential in a deaerated 0.1 M Na_2SO_4 solution containing 0.1 M each of $Fe(CN)_6^{3-}$ and $Fe(CN)_6^{4-}$ following the approach suggested by Cerquetti et al.[16].

RESULTS

The values of the potential for passivity breakdown, E_b, in deaerated, simulated ground water (pH 8.4) are plotted as a function of the chloride concentration and shown in Figure 1 for the three temperatures studied. It is seen that over the temperature range of 25 to 95 °C there was little variation of E_b with temperature for any given chloride concentration. All the data for tests in solutions with chloride concentrations ranging from 0.01 M to 4 M fit a linear logarithmic relationship, independent of temperature similar to that for E_{rp} as given by Eq. (1), where B and $E°_b$ were found to be equal to 131 mV/decade and 0.08 V_{SCE}(0.32 V_{SHE}) respectively. At a chloride concentration of 0.001 M (1mM), however, E_b is very high, exhibiting a significant deviation of the linear dependence on the logarithm of the chloride concentration presumably associated with the concomitant oxidation of water and the evolution of oxygen. A significant effect of pH on E_b was noted, with increasing pH leading to higher values for E_b. This effect, however, was attributed to the dependence of E_b on scan rate, in particular to the delayed initiation of pits in alkaline solutions (pH 8.4 and 10.7) as compared to the acidic solution [14,17].

As shown in Figure 2, a plot of E_{rp} as a function of chloride concentration for the tests conducted in the simulated ground water (pH 8.4) exhibits a similar independence of temperature as that observed for E_b. E_{rp} displayed a linear logarithmic dependence on chloride concentration, as described by Eq. (1), and similar to that shown in Figure 1 for E_b. However, the linear dependence extends to the lowest chloride

concentration. The values of B and $E°_{rp}$ are both lower than those for passivity breakdown and equal to 83 mV/decade and 0.04 V_{SCE} (0.28 V_{SHE}) respectively. The effect of solution pH (from 2.1 to 10.7) was relatively minor with respect to E_{rp}, and essentially negligible as previously reported [17].

To verify that E_{rp} can be used as a threshold potential for the occurrence of localized corrosion of Zr-4, a potentiostatic test was conducted in simulated groundwater containing 1.0 M NaCl at 95 °C and an applied potential of 0.055 V_{SCE}. This potential represents an overpotential of approximately 25 mV with respect to E_{rp} for the same chloride concentration. Upon the application of the potentiostatic step, the current density increased initially up to a value of the order of 3 mA/cm^2 prior to decaying to a steady state value of 0.75 mA/cm^2. The experiment was terminated after only 3 min of polarization because extensive attack was observed on the specimen surface. As noted after the CPP tests, pitting corrosion was localized outside the area defined by the crevice former and confined to the boldly exposed surfaces of the specimen.

Figure 3 shows the typical morphology of the localized corrosion of Zr-4 specimens exposed to chloride-containing simulated groundwater at 95 °C. The localized corrosion burrowed beneath the oxide layer cutting a shallow, irregularly shaped network of pits and leaving a thin film of oxide suspended above the pits. In more dilute chloride solutions the shallow, irregular network of pits exhibited a spider web or tree branch pattern on the exposed surfaces of the specimen. The most important observation, however, is the absence of detectable localized attack beneath the crevice former feet, even though this occluded geometry represents the most aggressive environmental condition for many passive metals and alloys [14]. Localized corrosion, in the form of shallow, covered pits, was confined to the boldly exposed specimen surfaces.

The conjoint effect of the other anions present in the simulated groundwater on the values of E_b and E_{rp} is illustrated in Figure 4. The data obtained in CPP tests conducted in deionized water containing only

0.001 M and 0.01 M NaCl at 25 °C indicate that the other anions and their concentration in the simulated groundwater [0.25 mM SO_3^{-2}, 0.16 mM NO_3^-, 0.10 mM F^-, and a total carbonate ($HCO_3^- + CO_3^{2-}$) concentration of 1.4 mM], have, with the exception of F^-, an inhibiting effect at the low chloride concentration because both E_b and E_{rp} increased with respect to the values obtained in pure chloride solutions, as shown in Figure 4. However, when the chloride concentration was increased to 1.0 M, the effect of these anion concentrations on E_b and E_{rp} became almost negligible.

Plots of the evolution of E_{corr} of as-polished and pre-oxidized Zr-4 in air saturated, simulated groundwater containing 1 M NaCl at 95 °C are shown in Figure 5. After 60 to 80 h of exposure to the solution, E_{corr} for the as-polished specimen was found to be approximately −0.30 V_{SCE}. Figure 5 shows that when 5 mM of hydrogen peroxide was added to the solution, to simulate the formation of hydrogen peroxide as the most stable product from the γ- radiolysis of water, there was a rapid increase in E_{corr}, followed by a slower decay to the original values. A repeat of the peroxide addition elicited a similar spike with the subsequent decay of E_{corr}. However, following the addition of 10 mM of ferric chloride ($FeCl_3$) at 160 h, E_{corr} increased rapidly exceeding E_{rp} and remained just above its value for the duration of the test (approximately 275 h). Examination of the specimen surface revealed the initiation of localized corrosion, in agreement with the observation that E_{corr} reached E_{rp}, which is equal to ~ 0.03 V_{SCE} in the 1 M NaCl solution.

The oxide film in the SNF cladding typically has a thickness which increases with average fuel rod burnup, ranging from 10 to 60 μm as a result of oxidation under service conditions [4]. To evaluate the effect of a thermally grown oxide film on the localized corrosion behavior of Zr-4, additional experiments were carried out using specimens oxidized in air. As-polished specimens were heated in air at 200 °C for 9 and 56 days. The specimens heated at 200 °C for 9 days exhibited an orange-yellowish oxide layer,

whereas the ones heated for 56 days showed a deep purplish-blue color. The oxide layers are estimated to be 84 and 154 nm thick respectively, as calculated using the oxide growth laws reported in the literature [18,19]. Only a slight decrease of E_b and E_{rp} with oxidation time at 200 °C was noted [17].

No corrosion under the crevice former was observed on the air-oxidized specimens after conducting the CPP tests. However, there was a significant change in the morphology of pitting corrosion, as compared to that observed on the polished specimens. Following the CPP tests, open, hemispherical pits with a heavily corroded bottom were detected on the specimen surface. Figure 6 shows a scanning electron micrograph of the surface of a 200 °C air-oxidized specimen exhibiting a typical pit with a diameter of approximately 260 μm and a depth of about 240 μm.

The evolution of the E_{corr} of an air-oxidized (at 200 °C for 9 d) specimen of Zr-4 in air saturated, simulated groundwater containing 1.0 M NaCl at 95 °C is shown in Figure 5. It is seen that E_{corr} stabilized at values close to −0.10 V_{SCE} after approximately 25 h. This value is about 300 mV higher than that corresponding to polished specimens. As in the test performed with the as polished specimen, 5 mM of hydrogen peroxide was added at 30 h to simulate the effect of radiolysis products. In this case, however, E_{corr} rapidly increased and exceeded E_{rp} by over 150 mV and remained at this value for the entire duration of the experiment (approximately 130 h). As mentioned above, the E_{rp} of an air oxidized specimen of Zr-4 in this environment was determined to be about 0.03 V_{SCE}. After the test, the initiation and propagation of pitting corrosion was confirmed in this specimen.

The relative electronic and electrochemical properties of the oxides formed in air in the as-polished and thermally at 200 °C for 9 days were examined using EIS and the oxidation/reduction kinetics of the $Fe(CN)_6^{3-}/Fe(CN)_6^{4-}$ redox couple was measured. The oxidation/reduction kinetics of the redox couple were studied to determine the relative electrical conductivity changes of the oxide films formed during

preoxidation. Figure 7 shows the Nyquist, Bode phase and magnitude plots for specimens covered by the different oxides after 24 h of polarization in the passive regime (–0.25 V_{SCE}) in deaerated 10 mM NaCl at 95 °C. As can be seen, the magnitude of the impedance increases with increasing oxide thickness. Similar results were observed with the $Fe(CN)_6^{3-}/Fe(CN)_6^{4-}$ couple in which the relative anodic and cathodic current densities are compared to form a basis as to the electronic properties of the oxides. It was found that the 200 °C oxide had approximately 10% of the conductivity of the as-polished film.

DISCUSSION

It has been reported that the critical potential for the initiation of pitting corrosion of Zr-4 in chloride solutions as measured using potentiodynamic polarization curves, exhibited a significant variability from test to test [20], undoubtedly related to the stochastic nature of pit initiation [21]. In addition, variability was found to be extremely dependent on surface preparation and scan rate [13]. For these reasons, CPP tests were used in this investigation to determine the E_{rp} for creviced specimens.

As shown in Figure 2, E_{rp} for Zr-4 exhibits a linear dependence on the logarithm of the chloride concentration that extends from concentrations of the order of mM to values close to NaCl saturation. The slope of this dependence, represented by B in Eq. (1), is approximately equal to 0.083 V/decade, a value similar to that reported by Maguire [11] and slightly higher than the theoretical value derived by Galvele in his model of pitting corrosion [15]. From the data shown in Figure 2 it can be inferred that both B and E^0_{rp} are independent of temperature practically up to the boiling point of water. This observation confirms and extends previous findings of Maguire [11] for pure Zr and reveals that Zr-4, contrary to the case of many metals and alloys [14,22], does not exhibit a decrease in E_{rp} and E^0_{rp} with increasing temperature in the range of 25 to 95 °C.

A value of E^0_{rp} equal to 0.04 V_{SCE} and independent of temperature was calculated by linear regression of the plot in Figure 2. This value is about 60 mV lower than that found by other authors in pure chloride solutions at room temperature [8,23]. The difference cannot be related to the anions present in the simulated ground water, because, as shown in Figure 4, their effect should be, if not negligible, just the opposite. The most reasonable explanation for the difference with respect to the literature data appears to be related to the method used to determine the value of E_{rp} from the CPP curves. As discussed elsewhere [17], if E_{rp} is estimated from the intersection of the forward current density with the approximately linear extrapolation of the reverse current density once pitting has been initiated, the value obtained could be 50 to 60 mV greater than that obtained through the intersection of the plotted curves. The bend in the reverse current density plot approaching the intersection with the forward current (Figure 8) may be the result of using a relatively fast potential scan rate, which introduces an error in the determination of E_{rp}. Nevertheless, the values reported in Figure 2 can be considered a lower bound for $E_{rp,}$ and therefore, can be used with confidence in long-term performance assessments.

The plot of E_b shown in Figure 1 also exhibits a linear dependence on the logarithmic of the chloride concentration which is independent of temperature but the values of E^o_b and B are significantly higher than those corresponding to repassivation. The difference between E_b and E_{rp}, and, as a consequence, between E^0_b and E^0_{rp}, is related to the stochastic nature of the pit initiation process and the deterministic character of repassivation once pit growth has occurred. Indeed, Mankowski et al. [20] have demonstrated that the initiation time for pitting of Zr-4 under potentiostatic conditions at potentials above E_{rp} obeys a log-normal distribution and the mean initiation time increases with decreasing potential. Therefore, if sufficient time is allowed for pit initiation to occur, the difference between E_b and E_{rp} tends to become negligible and justifies the use of E_{rp} as a useful threshold parameter for predicting the occurrence of localized corrosion [24]. The

difference in the value of B between initiation and repassivation, however, deserves additional discussion. The high value of B, equal to 0.131 V/decade for the expression of E_b corresponding to Eq. (1) suggests that the calculation of this important parameter for modeling pitting corrosion using results from CPP testing, as has been reported [14], may not be as useful because it is dominated by the random nature of the pit initiation process and therefore extremely dependent on experimental factors, such as surface roughness, potential scan rate, passivation times, and other test procedures. For example, Mankowski et al. [20] found that the initiation time increases with the decrease in surface roughness and with increases in the prepolarization time in the passive range.

The anions present in the groundwater at the proposed repository have a limited inhibiting effect on the pitting corrosion of Zr-4 as can be concluded from the plots of E_b and E_{rp} shown in Figure 4. Maraghini et al; [6] found that the strength of the inhibiting effect of these anions decreases in the order: $NO_3^- > SO_4^{2-} > HCO_3^-$. It is apparent, however, that the ratio of the sum of the weighted concentration of inhibitor anions (X^-) to chloride ion concentration is the important parameter to evaluate the inhibiting efficiency as illustrated in Eq. (2)

$$\frac{\sum a_i [X^-]_i}{[Cl^-]} > 1 \qquad (2)$$

where a_i is a weighted coefficient which is a measure of the inhibitory efficiency of the anion. Inhibition only occurs when this ratio is far greater than one. This is indeed the case for chloride concentrations equal to or less than 0.01 M, as shown in Figure 4, where both E_b and E_{rp} are higher in the solutions containing the anions present in the groundwater compared to that in the pure NaCl solutions.

The presence of a thermally formed oxide film grown at 200 °C covering the metal surface did not change significantly the values for E_b and E_{rp} [17], at least within the range of oxide film thickness investigated from pre-oxidation at this temperature. What is of importance is that the morphology of the localized attack changed substantially (Figure 6). It appears that deeper pits can develop as a result of the relative protection offered to the surrounding surface by the thin thermally grown film. This change in pit morphology is of technological significance in that the relative pit penetration rate is likely to be greater on the materials with a thermally grown oxide as compared to the as-polished materials. As such, the Zr cladding that has been previously exposed to reactor service which is known to have oxide films several tens of microns thick, may be more prone to suffer from hemispherical pits rather than the mottled attack observed for the as-polished material and as a result cladding breaches may be more rapid than is predicted based on testing of as-polished specimens. Further work examining this possibility on thicker hydro thermally grown films is therefore necessary and planned.

An additional important effect to consider relates to the role of hydrogen peroxide. It is assumed that reducible species generated by the radiolysis of water may increase the E_{corr} observed in air-saturated solutions above E_{rp}. In addition to unstable radicals, hydrogen peroxide is the most stable molecular species generated by water radiolysis. However, hydrogen peroxide seems to decompose rapidly in contact with a Zr-4 surface covered by the thin oxide film (about 4 to 6 nm thick) formed in aqueous solutions, as shown in Figure 5. On the contrary, when the Zr-4 surface is covered by the thermally formed oxide film no such decomposition takes place and a stable, higher E_{corr} is measured, as shown in Figure 5. In line with this, zircaloy metallic surfaces have been shown to catalyze the decomposition of H_2O_2 [25]. A possible explanation for this effect may be related to the electrochemical decomposition of H_2O_2 through its own coupled redox reactions. If the growth of a thermally formed film affects the electronic conduction path

through the intermetallic particles existing in Zr-4 [3,26], it is possible that the autocatalytic decomposition of H_2O_2 is slowed down. As a result, the potential will continuously rise until a steady state value of E_{corr} is reached, as illustrated in Figure 5. It can be noted that prior to the addition of H_2O_2, E_{corr} is higher in the pre-oxidized specimen than in the polished specimen with the film formed in air at room temperature. This is an additional indication that the balance between the kinetics of the anodic and cathodic reactions determining E_{corr} has been modified by the thermally grown film. This, presumably, is due to an increase of the potential required for the cathodic reduction of oxygen to attain a current equal to that of the passive dissolution of Zr-4, which is lower on the alloy covered by the thermally grown oxide. Thus, there appears to be two competing effects which influence E_{corr}. A decrease in the cathodic kinetics on the thermally grown oxide which should result in a decrease in E_{corr}. This decrease is counter balanced by a decrease in the passive dissolution rate that would result in an increase in E_{corr}, which is evidently larger resulting in a net increase in E_{corr}.

This interpretation is further supported by the results obtained using EIS and current measurements of the couple $Fe(CN)_6^{3-}/Fe(CN)_6^{4-}$. When the EIS results were fitted using a simple RC parallel circuit to model the response of the oxide film [27-29] as indicated by the solid lines in Figure 7, the film resistance as a function of time in the passive range for the thermally grown oxides was relatively constant after 5 h exposure, whereas the resistance of the as-polished oxide asymptotically approached steady state over more extended exposure times (Figure 9). Though clearly an oversimplification for the nature and structure of the oxide, the results obtained with this model indicate that there is a significant difference in the resistance of the thermally grown oxide compared to the as-polished film and are in line with the results reported by others [27] including those who used more complicated models for the oxide film on Zr-4 [30]. It should also be noted that other, more complex models were examined, however the results obtained

using the simple model proposed here provided the best fit to the experimental data. The film capacitance was free to vary during the fitting routine, however no appreciable difference in the capacitance as a function of time was observed. There was a significant difference in the capacitance of each oxide, with a ratio of the as-polished to the 200 °C oxide of approximately 0.17 in agreement with the notion that the film thickness and resistance increases with increasing pre-oxidation. The relative electronic conductance of the respective oxides found by comparing the anodic and cathodic currents associated with the $Fe(CN)_6^{3-}/Fe(CN)_6^{4-}$ couple also supported the view of enhanced decomposition of H_2O_2 on the as-polished oxide compared to the thermally grown oxide by comparing the relative electronic conductivity of these films as measured in the oxidation/reduction kinetics. These tests showed that the thermally grown oxide at 200 °C for 9 days had approximately 10 of the conductivity (or 10 × the resistance) of the air-formed film, which is nearly qualitatively the same as the results from EIS.

As the chloride concentration in the solution increased to values close to the solubility of NaCl, E_{rp} decreased to near 0.0 $V_{SCE,}$ as shown in Figure 2. This indicates that localized corrosion of Zr-4 is likely to occur if this range of chloride concentration is attained in the presence of oxidizing species such as radiolysis products or reducible cationic species (i.e., Fe^{3+}) arising from the corrosion of carbon steel baskets used inside WPs to maintain the fuel assemblies in position. It is not known if these conditions, in terms of availability of reducible species at a sufficiently high concentration, are likely to occur in the environment in contact with the Zr-4 spent fuel cladding in the proposed repository. If this is the case, the possibility of localized corrosion needs to be evaluated further. As noted in Figure 5 the addition of $FeCl_3$ also increases E_{corr} above E_{rp} and can lead to the initiation of localized corrosion, as is well documented in the case of Zr [11,31]. Nevertheless, Fe^{3+} cations may not be available in sufficiently high concentrations

if the pH of the WP internal environment is buffered by the presence of relatively high concentrations of HCO_3^- anions which may result in precipitation of ferric oxyhydroxides.

The results of this study have clearly shown that Zr-4 is more resistant to crevice corrosion than to pitting corrosion, contrary to the case of many corrosion resistant alloys such as stainless steels and Ni-Cr-Mo alloys in which the passive behavior is related to the presence of a Cr-rich passive film. The preferential occurrence of pitting corrosion on boldly exposed surfaces, rather than in the tight crevice existing on the specimens, can be explained because Zr does not exhibit an active loop even in concentrated HCl solutions as stainless steels and Ni-base alloys do. As a consequence, the metal surface inside the crevice region remains passive without the localized depassivation usually caused by the simultaneous action of high concentrations of H^+ and Cl^- ions. In this regard Zr is very similar to Ta [32], which also exhibits resistance to crevice corrosion and lacks an active loop in strong acid solutions. No simple explanation exists for this behavior, and additional studies on the stability of metastable pits under crevice and no-crevice conditions are required.

CONCLUSIONS

1. Zr-4 is susceptible to pitting corrosion in chloride-containing solutions at concentrations above 0.001M and potentials higher than a critical potential which depends linearly on the logarithm of the chloride concentration but is temperature independent.
2. The repassivation potential can be adopted as a lower bound for the critical potential for pitting corrosion.
3. No crevice corrosion is observed under the same environmental and electrochemical conditions that promote pitting corrosion.

4. Although the presence of a thin (a few 100 nm) thermally grown oxide film does not affect the value of the repassivation potential, it promotes a significant increase in the corrosion potential in both air-saturated and H_2O_2-containing solutions and changes the morphology of the attack.

5. The corrosion potential in some cases can reach the repassivation potential in solutions containing H_2O_2 and therefore pitting corrosion of Zr-4 fuel cladding may occur under natural corroding conditions inside a breached container.

ACKNOWLEDGMENTS

This investigation was conducted with the support of Nuclear Regulatory Commission under Contract No. NRC-02-97-009. The paper presents the opinions of the authors and in no way is intended to reflect or represent the views or regulatory position of the US Nuclear Regulatory Commission. The technical assistance provided by S. Clay and F. Daby (Southwest Research Institute) is gratefully appreciated.

REFERENCES

1. Federal Register, v. 64, n. 34, February 22, 1999.

2. U.S. Department of Energy, Viability Assessment of a Repository at Yucca Mountain, Overview and all five volumes. DOE/RW–0508. Las Vegas, NV: U.S. Department of Energy, Office of Civilian Radioactive Waste Management (1998).

3. B. Cox, in Advances in Corrosion Science and Technology, M. Fontana and R.W. Staehle, eds. New York, NY: Plenum Press. Vol. 5, 173 (1976).

4. B. Cox, in Third International Symposium on Environmental Degradation of Materials in Nuclear Power Systems - Water Reactors, Warrendale, PA: The Metallurgical Society: 65 (1988).

5. D.G. Franklin and P.M. Lang, in Ninth International Symposium of Zirconium in the Nuclear Industry. C.M. Eucken and A.M. Garde, eds. ASTM STP 1132. Philadelphia, PA: American Society for Testing and Materials: 3 (1991).

6. M. Maraghini, G.B. Adams, Jr., and P. Van Rysselberghe, *J. Electrochem. Soc.* 101: 400 (1954).

7. Ya.M. Kolotyrkin, *J. Electrochem. Soc.* 108: 209 (1961).

8. G. Cragnolino and J.R. Galvele, in Passivity of Metals, R.P. Frankenthal and J. Kruger, eds., Princeton, NJ: The Electrochemical Society: 1,053 (1978).

9. D.R. Knittel, M.A. Maguire, A. Bronson, and J.-S.Chen, *Corrosion* 38: 265 (1982).

10. D.R. Knittel and A. Bronson, *Corrosion* 40: 9 (1984).

11. M. Maguire, in Industrial Applications of Titanium and Zirconium: Third Conference, R.T. Webster and C.S. Yong, eds ASTM STP 830, Philadelphia, PA: American Society for Testing and Materials: 175 (1984).

12. J. Jangg, R.T. Webster, and M. Simon, *Werkstoffe und Korrosion* 29: 16 (1978).

13. G.A. Cragnolino, D.S. Dunn., C.S. Brossia, V. Jain, and K.S. Chan, Assessment of Performance Issues Related to Alternate Engineered Barrier System Materials and Design Options, CNWRA 99-003, San Antonio, TX: Center for Nuclear Waste Regulatory Analyses (1999).

14. Z. Szklarska-Smialowska, Pitting Corrosion of Metals, Houston, TX: NACE International (1986).

15. J.R. Galvele, *J. Electrochem. Soc.* 123: 464 (1976).

16. A. Cerquetti, F. Mazza, and M. Vigano, in Localized Corrosion, NACE-3, R.W. Staehle, B.F. Brown, J. Kruger, A. Agarwal, eds., Houston, TX: NACE International: 661 (1974).

17. C.A. Greene, C.S. Brossia, G.A. Cragnolino, and D.S. Dunn, Paper no. 210, Corrosion2000, Houston, TX: NACE International (2000).

18. A. Rothman, Potential Corrosion Degradation Mechanisms of Zircaloy Cladding on Spent Nuclear Fuel in a Tuff Repository. UCID–20172. Livermore, CA: Lawrence Livermore National Laboratory (1984).

19. J. Clayton and R. Fischer, in Proceedings of the American Nuclear Society Topical Meeting on Light Water Reactor Fuel Performance. LaGrange Park, IL: American Nuclear Society: 1: 1 (1985).

20. G. Mankowski, Y. Roques, G. Chatainier, and F. Dabosi, *Brit. Corr. J.* 19: 17 (1984).

21. G. Mankowski, P.Eygazier, Y. Roques, G. Chatainier, and F. Dabosi, in Passivity of Metals and Semiconductors, Amsterdam, The Netherlands: 299 (1983).

22. G.A. Cragnolino, in Advances in Localized Corrosion, H. Isaacs, U. Bertocci,. J. Kruger, and S. Smialowska, eds. Houston, TX: NACE International: 413 (1990).

23. B. Cox, *Corrosion* 29: 157 (1973).

24. D.S. Dunn, N. Sridhar, and G.A. Cragnolino, *Corrosion* 52: 115 (1996).

25. Waterside Corrosion of Zirconium Alloys in Nuclear Power Plants, IAEA-TECDOC-996, International Atomic Energy Agency, 220 (1998).

26.. J.B. Van der Sande, and A.L. Bement, *J. of Nuclear Mat.* 52:115 (1974).

27. M.M. Al-Abdallah, *Anti-Corrosion Methods and Materials* 43: 17 (1996).

28. W.A. Badawy and F.M. Al-Kharafi, *Bull. Electrhochem.* 12: 505 (1996).

29. P.M. Rosecrans, in Zirconium in the Nuclear Industry, D.G Franklin and R.B. Adamson, eds. ASTM STP 824, Philadelphia, PA: American Society for Testing and Materials: 531 (1984).

30. O. Gebhardt, M. Gehringer, Th. Graber, and A. Hermann, *Mat. Sci. Forum* 192–194: 587 (1995).

31. T.-L. Yau and R.T. Webster, in Metals Handbook. Volume 13 Corrosion. Materials Park, OH: ASM International: 707–721 (1987).

32. M. Schussler and C. Pokross, in Metals Handbook. Volume 13 Corrosion. Materials Park, OH: ASM International: 724–739 (1987).

TABLES

TABLE 1
Composition of Zr-4 utilized in current study (in wt %)

Sn	Fe	Cr	Ni	O (ppm)	Zr
1.51	0.20	0.10	0.0035	1420	bal.

Figure Captions

Figure 1: Breakdown potentials for Zr-4 as a function of the chloride concentration simulated groundwater; $E_b (V_{SCE}) = 0.079 - 0.131 \log [Cl^-]$.

Figure 2: Repassivation potentials for Zr-4 as a function of the chloride concentration simulated groundwater; $E_{rp} (V_{SCE}) = 0.038 - 0.083 \log [Cl^-]$.

Figure 3: SEM micrograph showing typical pitting morphology observed after polarization of Zr-4 in chloride containing solutions.

Figure 4: Breakdown and repassivation potentials measured in solutions with (open symbols) and without (filled symbols) the additional anions that are present in the groundwater near the proposed MGR. The additional anions and their concentrations are: 0.25 mM SO_4^{2-}, 0.16 mM NO_3^-, 0.10 mM F^- and a $HCO_3^- + CO_3^{2-}$ concentration of 1.4 mM.

Figure 5: Effect of H_2O_2 and $FeCl_3$ additions as well as pre-oxidation on the open circuit behavior of Zr-4 in air-saturated simulated groundwater containing 1 M NaCl at 95 °C.

Figure 6: SEM micrograph showing morphology of corrosion attack after polarization of a Zr-4 specimen pre-oxidized in air at 200 °C prior to polarization. The pit shown is roughly hemispherical, having a diameter of ~ 260 μm and a depth of ~ 240 μm.

Figure 7: EIS results for as-polished and 200 °C for 9 days, oxides in deaerated 10 mM NaCl at 95 °C after 24 h of polarization in the passive regime. The applied potential was -0.25 V_{SCE} for the as-polished and 200 °C oxides. Also shown on the figure (solid lines) are the result from fitting the data to a simple RC parallel circuit to model the oxide film.

Figure 8: Potentiodynamic polarization curve for Zr-4 in deaerated, simulated J-13 well water (pH 8.4) containing 1 mM NaCl at 95 °C. A scan rate of 0.167 mV/s was used. Note the possible differences depending whether the intersection of the forward and reverse scans or extrapolation prior to the decrease is used.

Figure 9: Oxide film resistance as calculated using the RC parallel circuit as a function of polarization time in the passive region for the as-polished, and 200 °C for 9 days oxides in deaerated 10 mM NaCl at 95 °C.

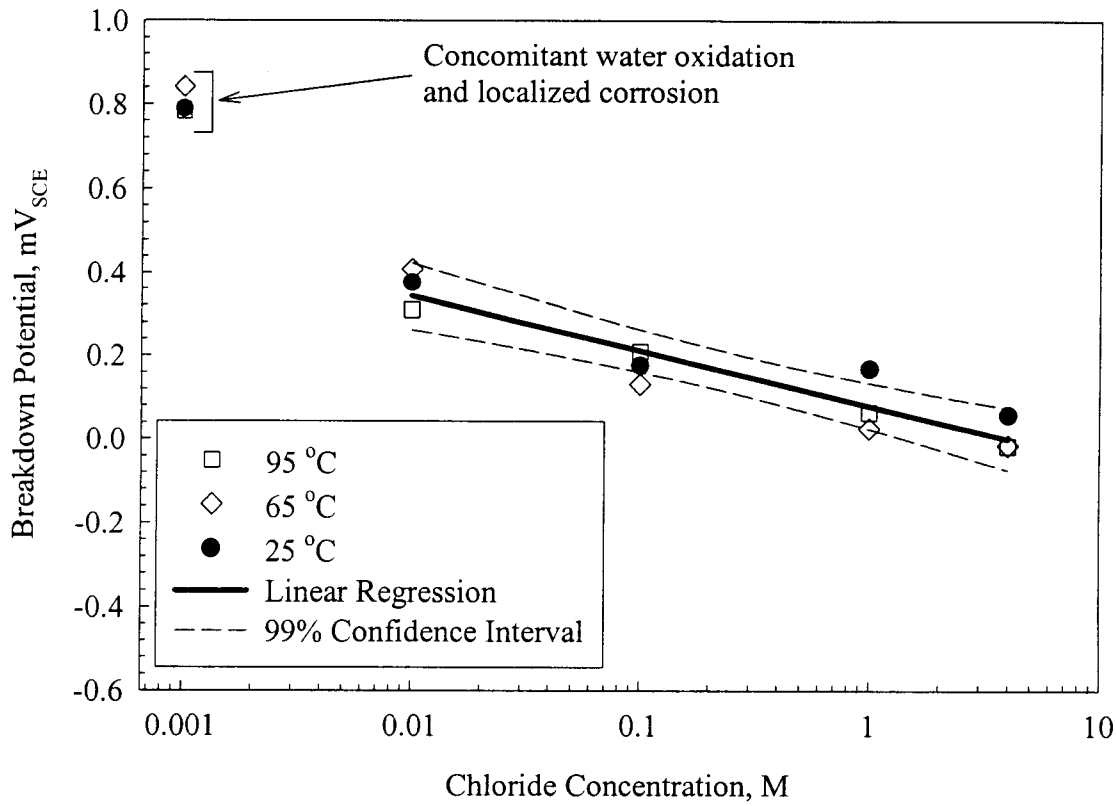
Concomitant water oxidation
and localized corrosion
Breakdown Potential, mV$_{SCE}$
1.0
0.8
0.6
0.4
0.2
0.0
-0.2
-0.4
-0.6
0.001
0.01
0.1
1
10
Chloride Concentration, M
95 °C
65 °C
25 °C
Linear Regression
99% Confidence Interval

Figure 1

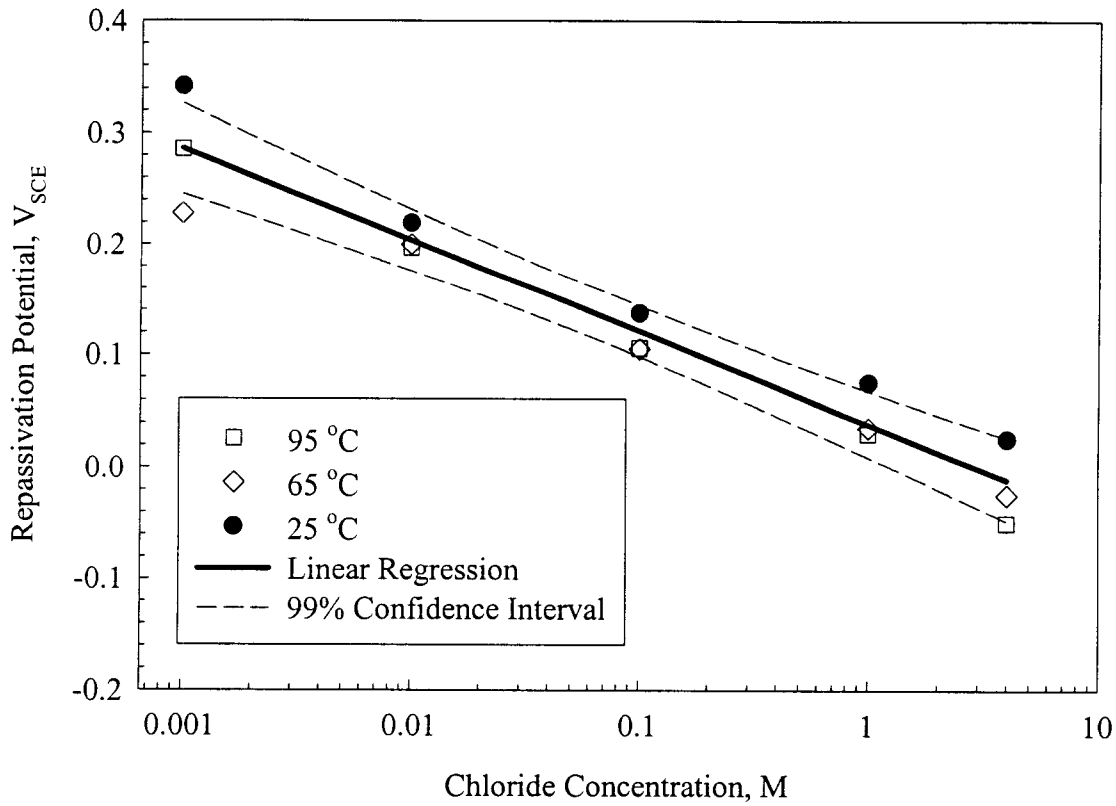
0.4
0.3
0.2
0.1
0.0
-0.1
-0.2
Repassivation Potential, V_{SCE}
0.001
0.01
0.1
1
10
Chloride Concentration, M
95 °C
65 °C
25 °C
Linear Regression
99% Confidence Interval

Figure 2

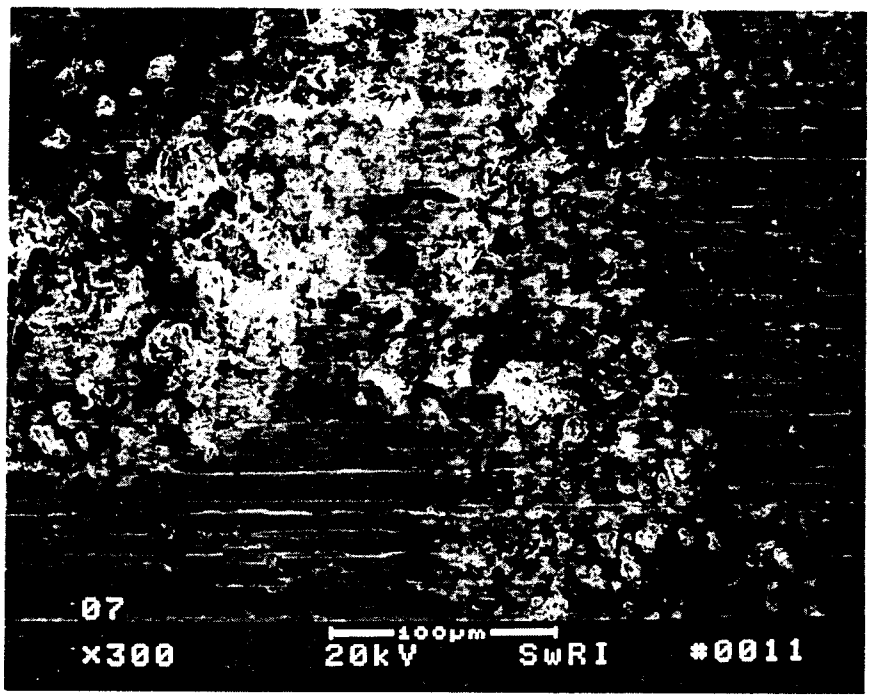

Figure 3

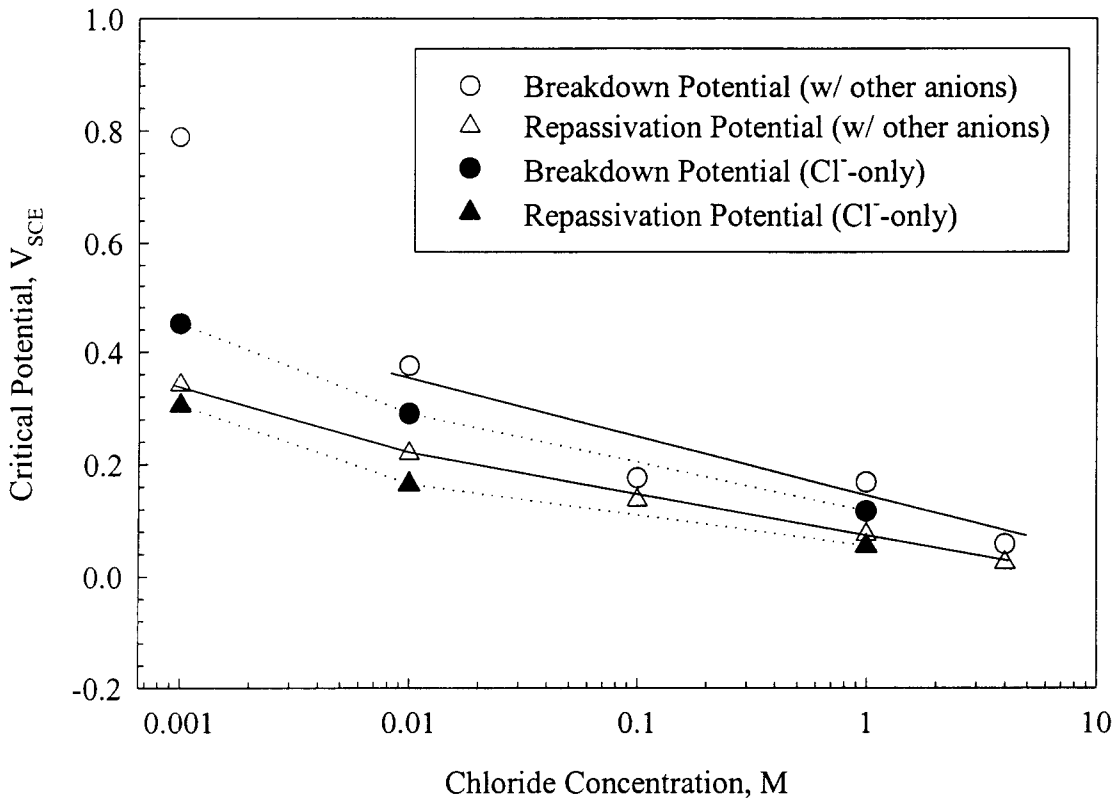
1.0
0.8
0.6
0.4
0.2
0.0
-0.2
Critical Potential, V_{SCE}
0.001
0.01
0.1
1
10
Chloride Concentration, M
Breakdown Potential (w/ other anions)
Repassivation Potential (w/ other anions)
Breakdown Potential (Cl^--only)
Repassivation Potential (Cl^--only)

Figure 4

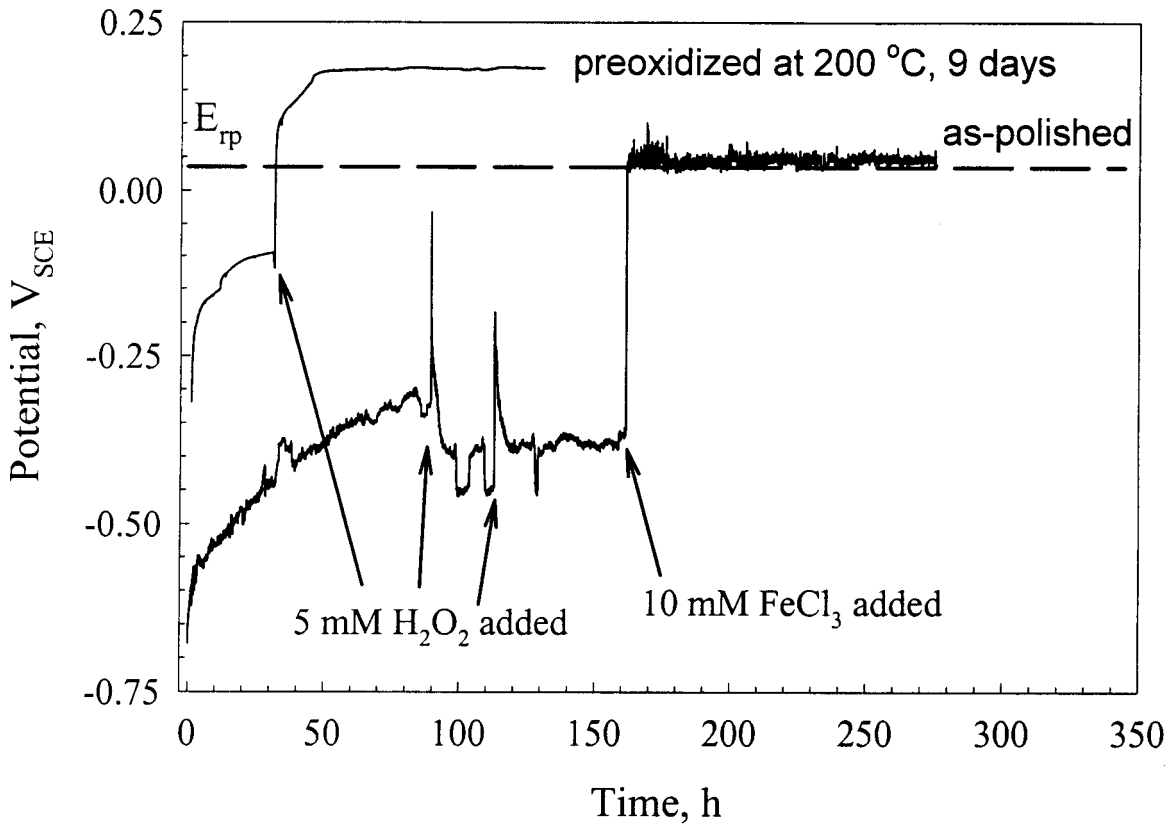
0.25
0.00
-0.25
-0.50
-0.75
Potential, V_{SCE}
0
50
100
150
200
250
300
350
Time, h
preoxidized at 200 °C, 9 days
E_{rp}
as-polished
5 mM H_2O_2 added
10 mM $FeCl_3$ added

Figure 5

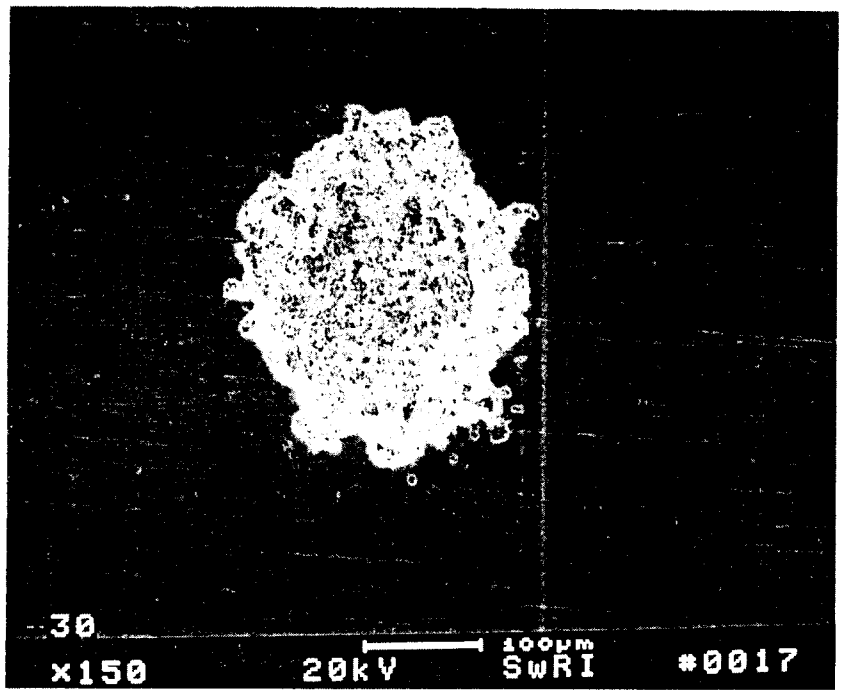

Figure 6

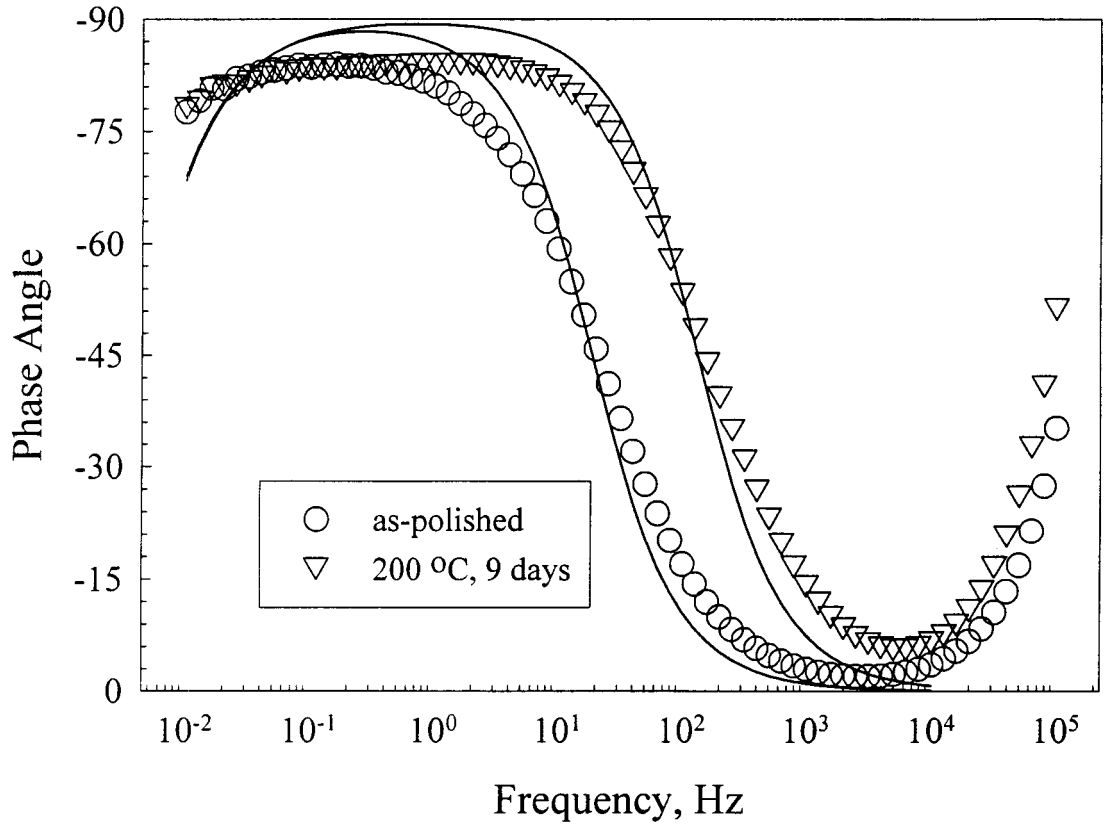
-90
-75
-60
-45
-30
-15
0
Phase Angle
as-polished
200 °C, 9 days
10-2
10-1
100
101
102
103
104
105
Frequency, Hz

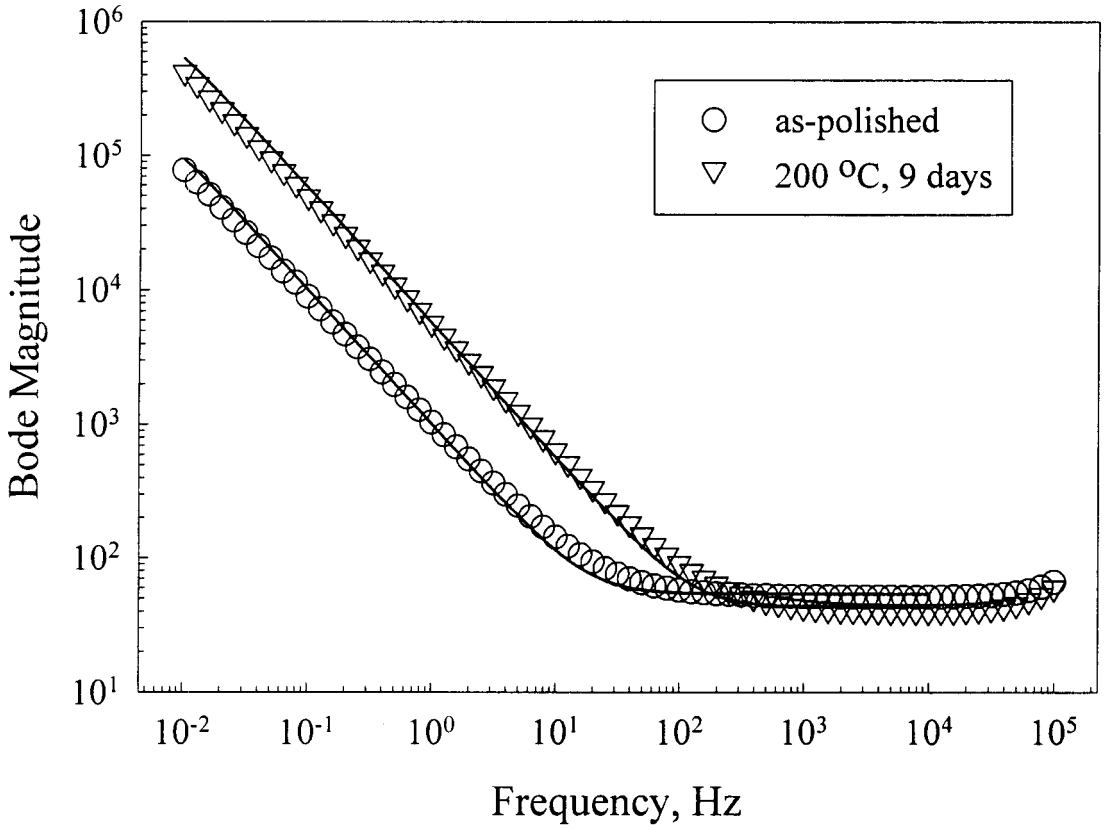
106
105
104
103
102
101
Bode Magnitude
as-polished
200 °C, 9 days
10-2
10-1
100
101
102
103
104
105
Frequency, Hz

Figure 7

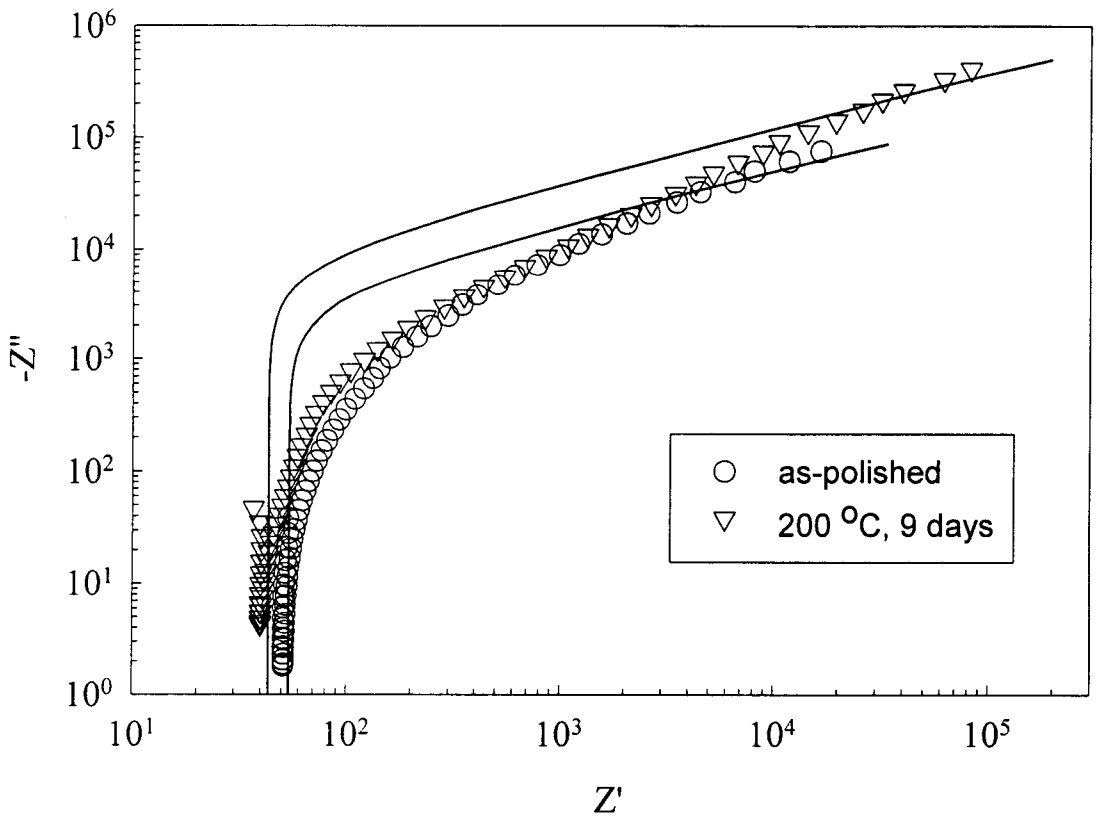

Figure 7 (cont)

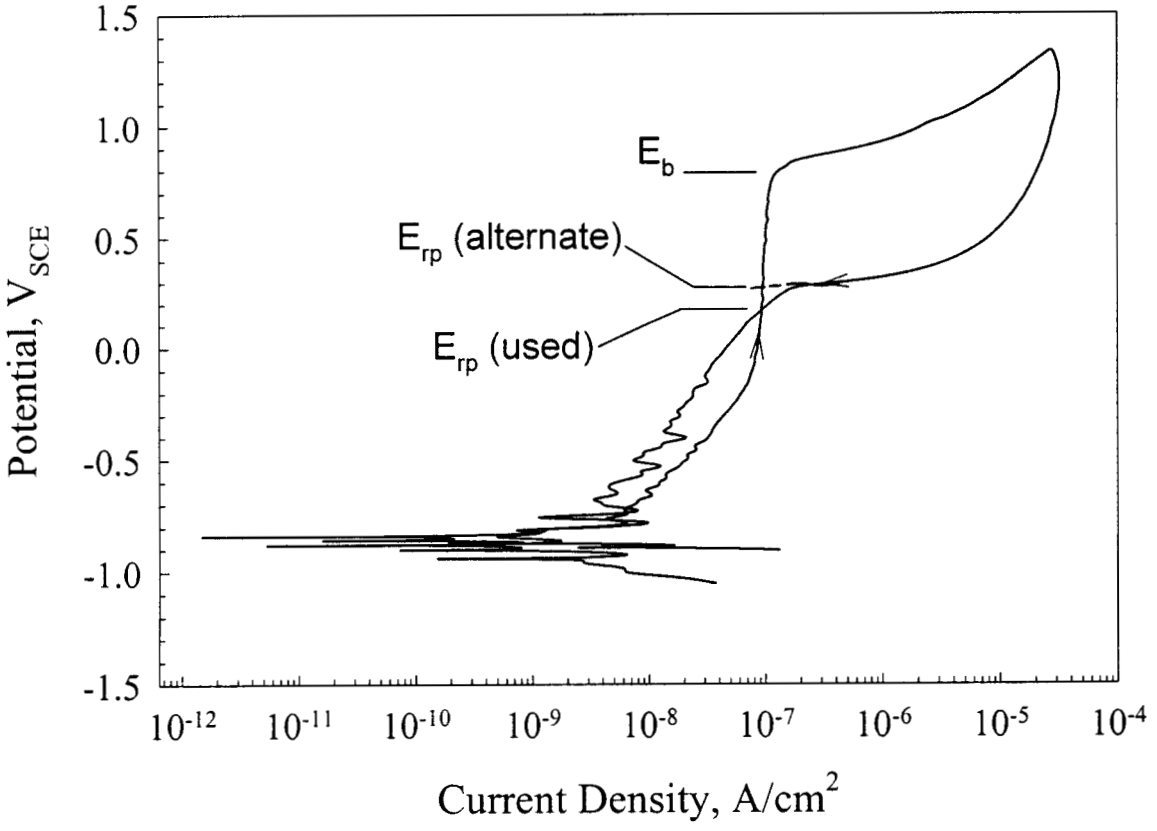
1.5
1.0
0.5
0.0
-0.5
-1.0
-1.5
Potential, V_{SCE}
E_b
E_{rp} (alternate)
E_{rp} (used)
10^{-12}
10^{-11}
10^{-10}
10^{-9}
10^{-8}
10^{-7}
10^{-6}
10^{-5}
10^{-4}
Current Density, A/cm^2

Figure 8

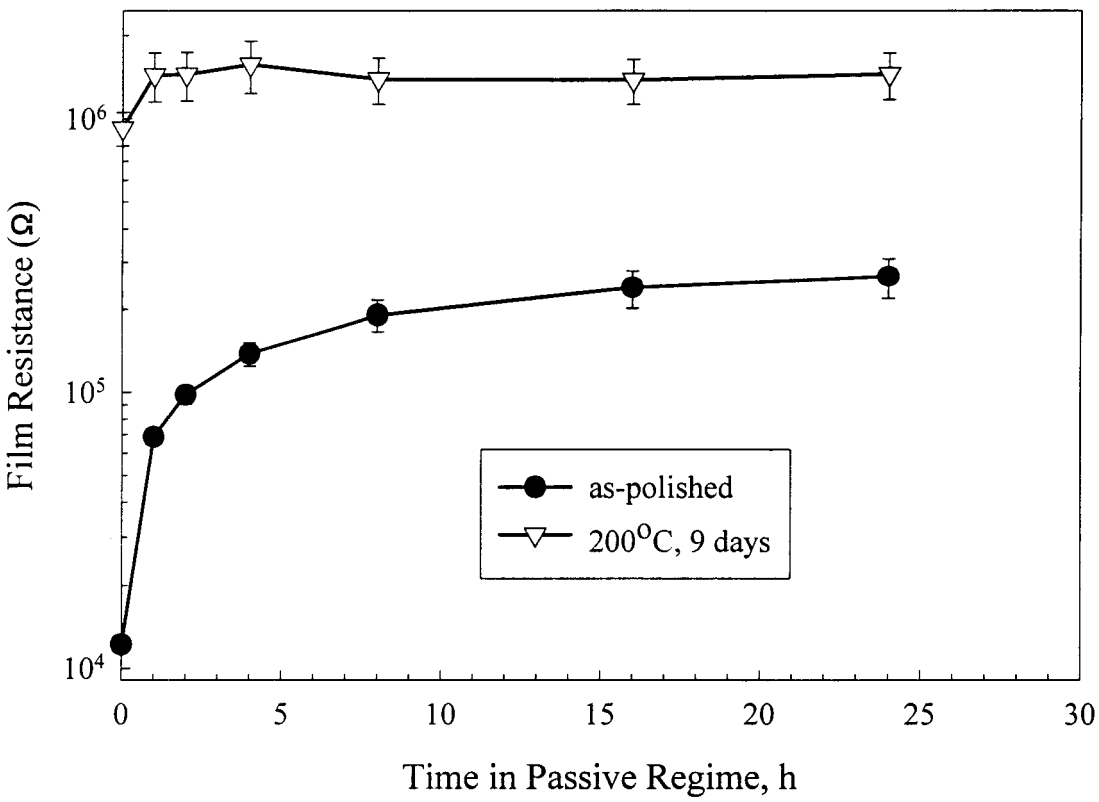
Film Resistance (Ω)
10^6
10^5
10^4
0
5
10
15
20
25
30
Time in Passive Regime, h
as-polished
200°C, 9 days

Figure 9